Influence of specimen geometry on measures of local fracture strain obtained from uniaxial tensile tests of AHSS sheets

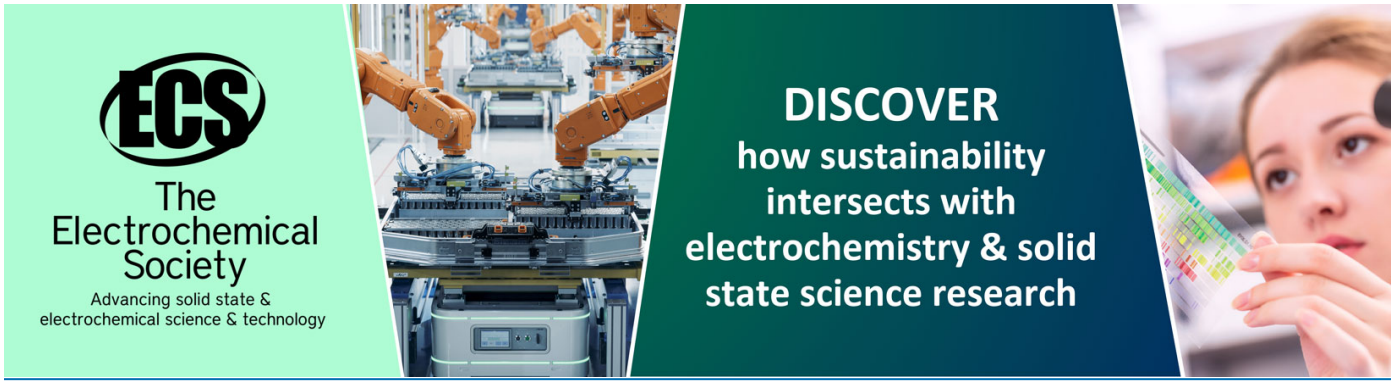

IOP Conf. Series: Materials Science and Engineering **418** (2018) 012074 doi:10.1088/1757-899X/418/1/012074

Influence of specimen geometry on measures of local fracture strain obtained from uniaxial tensile tests of AHSS sheets

L. Wagner[1], P. Larour[1]

[1] voestalpine Stahl GmbH, R&D – R&D Forming Technologies
voestalpine- Strasse 3, A-4020 Linz, Austria.

E-mail: leopold.wagner@voestalpine.com

Abstract. Enhanced formability mapping, based on parameters derived from uniaxial tensile tests, has been proposed in order to distinguish between local versus global formability of AHSS sheets. The assessment of fracture surfaces represents the basis of local formability indices, i.e. local fracture strains. Different specimen geometries as well as evaluation methods can be found in uniaxial tensile test standards. It is not yet clear whether the choice of test specimen or evaluation method influences the measures of local fracture strain. This paper aims at contributing to the ongoing discussion on these issues during enhanced formability mapping of AHSS grades. In this study two AHSS grades have been investigated in two thicknesses (t=1.5mm & 3.0mm). Besides standardized test specimens, the widths w of tensile test specimens were deliberately varied to gain custom tensile test specimens, exhibiting widths of 3.0mm, 6.0mm, 15.0mm and 30.0mm. The resulting measures of local fracture strain were related to the respective width-to-thickness ratio w/t as well as to the respective evaluation method. Distinct trends of all local fracture strains with respect to the w/t ratio could be detected. However, these trends tend to level off for certain w/t ratios, depending on the respective strain hardening behaviour of the investigated AHSS grade. For thicknesses up to 2mm standardized geometries with w larger than 20mm may be used indifferently. For higher thicknesses, e.g. for hot rolled AHSS grades, care has to be taken to choose the tensile specimen accordingly. Local fracture strain measures based on the actual fracture surface tend to show less variability and less dependence on the assessment method as compared to measures representing fracture thickness only. The overall trends as well as outliers depicted in the variability of results were discussed with respect to the fracture surface assessment methods.

1. Introduction

The wide range of mechanical properties of available advanced high strength steel (AHSS) grades represents a challenge when it comes to material selection during the design process of components formed from AHSS sheets. To facilitate material selection, enhanced formability mapping methods are needed, going beyond the commonly known representations of tensile elongation versus tensile strength (i.e. the classical “banana diagrams”). Possibilities to perform such an advanced formability mapping, based on parameters derived from standard uniaxial tensile tests, have been proposed [1, 2]. These mapping methods distinguish between the local ductility, needed e.g. for bending or hole expansion, and global ductility which is essential for e.g. deep drawing of AHSS sheets. Global ductility parameters are e.g. uniform elongation *UE* or tensile elongation *TE* determined from the

global stress-strain response. Local ductility measures are local fracture strain measures e.g. the reduction of area *Z*, true fracture strain (*TFS*) or true thickness strain (*TTS*). The potential of local ductility measures for material characterization has been highlighted by considerations to include such measures of local ductility into industrial material specifications, e.g. VDA 239-100 [3]. The concept of local versus global formability has also been recently discussed in the WorldAutoSteel AHSS guidelines handbook [4] and is therefore of increasing relevance for end users of AHSS steel grades.

The basis of local ductility indices lies in the assessment of the fracture surface after a tensile test. However, different specimen geometries can be found in test standards for uniaxial tensile testing of sheet metal, i.e. DIN EN ISO 6892-1 [5], ASTM E8 [6] or JIS Z 2241 [7]. These specimen geometries differ in their test length and more importantly in their specimen width, which has – together with the sheet thickness – a strong influence on the necking behavior and the stress state just before fracture [8], i.e. the extent of deviation of local strain paths in the necking zone from uniaxial tension towards plane strain prior to fracture. This will possibly affect all local ductility measures. Thus, following geometrical considerations, the width-to-thickness ratio *w*/*t* is likely to be the relevant parameter, characterizing tensile specimen geometries. It is not yet clear to which extent the choice of test specimen influences the measures of local fracture strains. It is also not clear whether a possible influence of specimen geometry may in addition rely on the mechanical properties of the investigated steel grade itself, e.g. the yield strength or the strain hardening behavior. This contribution aims at clarifying the issue of specimen geometry during uniaxial tensile test-based formability mapping of AHSS grades. Tensile tests are performed on different AHSS grades for two thicknesses, using standardized as well as customized specimen geometries to study the influence of *w*/*t*. Different measures of local fracture strain are related to *w*/*t*, giving a perspective of the respective performance of standardized specimen geometries and evaluation methods.

2. Materials, Methods and Definitions

2.1. Steel Grades

The chosen steel grades represent an upper and lower bound of AHSS/UHSS with respect to their ultimate tensile strength and their strain hardening behavior, especially at high plastic strains (>UE). Two cold rolled steel grades have been chosen for this investigation, namely DP600-CR and CP1200-CR. The investigation covers different thicknesses, namely 1.5mm as well as 3.0mm. In order to be able to test sheets with $t \geq 3.0$mm, equivalent available hot rolled grades had to be chosen, namely DP600-HR and MS1300-HR. The actual thicknesses differ slightly from the target thicknesses of 1.5mm and 3.0mm due to material availability (CP1200-CR: 1.52mm, DP600-CR: 1.42mm, MS1300-HR: 3.04mm, DP600-HR: 3.25mm).

2.2. Specimen Geometries

The cold rolled sheets were tested using three different specimen geometries (No. 1,2,3) described in DIN EN ISO 6892-1 [5] Annex B, exhibiting widths of 12.5mm, 20.0mm, and 25.0mm, respectively (Table 1). The hot rolled sheets were tested using a non-proportional specimen geometry described in DIN EN ISO 6892-1 [5] Annex D with a width w of 20.0mm (Table 1). The resulting *w*/*t* ratios are shown in Table 2, respectively.

Table 1. Specimen geometries used within this study: DIN B 1-3… DIN6892-1 Annex B No. 1-3, DIN D…DIN6892-1 Annex D, W3-30…customized samples (w_0…test width, L_0…test length, L_C…parallel length, t…tested thicknesses for each geometry).

	DIN B 1	DIN B 2	DIN B 3	DIN D	W3	W6	W15	W30
w_0 [mm]	12.5	20.0	25.0	20.0	3.0	6.0	15.0	30.0
L_0 [mm]	50	80	50	50	80	80	80	80
L_C [mm]	75	120	60	65	120	120	120	120
t [mm]	1.5	1.5	1.5	3.0	1.5/3.0	1.5/3.0	1.5/3.0	1.5/3.0

To increase the range of investigated specimen widths, all sheets have been tested using a special set of tensile specimen geometries. These are loosely based on the DIN EN ISO 6892-1 B No.2 geometry, but with altered specimen width. Widths of these specimens were 3mm (W3), 6mm (W6), 15mm (W15), and 30mm (W30), respectively (geometries in Table 1, w/t ratios in Table 2). The tensile tests were performed in longitudinal direction (according to VDA 239-100 [3]) using 3 parallel samples and testing conditions (strain rate, ambient conditions) described in DIN EN ISO 6892-1 [5].

Table 2. Resulting width-to-thickness ratios *w/t* for all tested specimens and steel grades (DIN B 1-3… DIN6892-1 Annex B No. 1-3, DIN D…DIN6892-1 Annex D, W3-30…customized samples).

	DIN B 1	DIN B 2	DIN B 3	W3	W6	W15	W30
DP600-CR	8.9	14.2	17.7	2.2	4.3	10.7	21.4
CP1200-CR	8.3	13.2	16.4	2.0	4.0	9.8	19.9
		DIN D		W3	W6	W15	W30
DP600-HR		6.1		0.9	1.8	4.6	9.1
MS1300-HR		6.7		1.0	2.0	5.0	9.9

2.3. Fracture Surface Assessment

Images of the fracture surface have been taken by means of a stereo-light-microscope (Zeiss Stemi 508) equipped with a digital camera (Zeiss Axiocam 105 color) with the fracture surface oriented perpendicular to the viewing direction of the microscope. According to ASTM E8 [6] thickness measurements were performed on the left and right edge of the fracture surface, t_{fLEFT} & t_{fRIGHT}, as well as in the middle of the fracture surface t_{fMID} (Figure 1a,b). Not all specimens had fracture cross sections of parabolic shape (Figure 1b). The minimum fracture thickness across the whole fracture surface t_{fMIN} is no longer identical to t_{fMID} and was determined as well. The width of the fracture surface w_{f} was either measured once in the middle of the thickness direction (Figure 1a,b) and projected back to the plane perpendicular to the tensile direction by means of the fracture angle α_{f} (Figure 1c), or measured from an image of the joined fractured specimens (Figure 1c). The fracture surface area was calculated according to:

$$A_{\mathrm{ASTM}} = w_{\mathrm{f}} * (t_{\mathrm{fLEFT}} + 4 * t_{\mathrm{fMID}} + t_{\mathrm{fRIGHT}})/6 \quad (1)$$

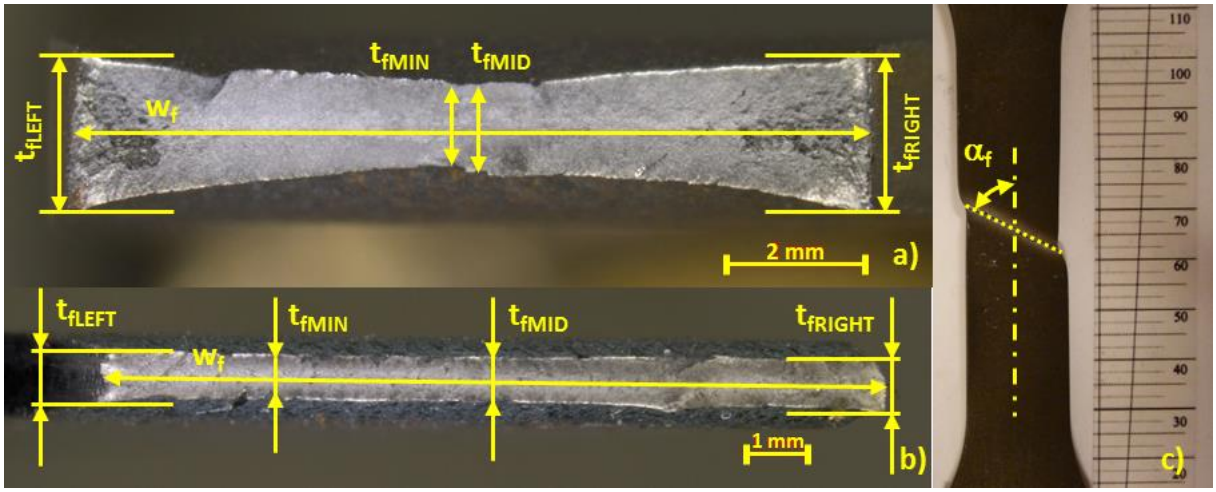

Figure 1. Fracture surface assessment – width and thickness measurements in the fracture surface (a,b) as well as fracture angle determination (c).

An alternative fracture surface assessment method performed is as well, where A_{fContour} is directly determined by identifying the contour of the fracture surface and calculating the integrated area within a bounding polygon. This bounding polygon was determined manually, closely following the contour,

i.e. largest point distance on the contour was typically <0.1mm. The area is then projected back to the plane perpendicular to the tensile direction by means of the fracture angle α_f.

2.4. Local Fracture Strain Measures

Different measures of local ductility were derived from the assessment of the fracture surface of the respective tensile specimens. These measures include:

- reduction of area at fracture $Z = (A_0 - A_f)/A_0$ (2)
- true fracture strain $TFS = \ln(A_0/A_f) = \ln(1/(1-Z))$ (3)
- true thickness strain $TTS = \ln(t_f/t_0)$ (4)
- true width strain $TWS = \ln(w_f/w_0)$ (5)

with t_0, w_0 and A_0 as initial thickness, width and cross section as well as t_f, w_f and A_f as thickness, width and cross section at fracture. Z and TFS are calculated by using A_{fASTM} and $A_{fContour}$ whereas TTS is calculated using t_{fMID}, t_{fMIN} and $t_{fMEAN} = (t_{fLEFT} + 4 * t_{fMID} + t_{fRIGHT})/6$.

3. Results and Discussion

The first observation was a change in fracture type from a cup-and-cone fracture pattern via a through-thickness shear fracture towards across-width shear fracture pattern with increasing w/t (Figure 2). The transition to shear fracture across the specimen width seems to depend on the tested steel grade, i.e. on its strain hardening behaviour [8]. It turns out to lie at w/t_{CRIT} of 4-5 for CP1200/MS1300 and w/t_{CRIT} of 8-9 for DP600. The fracture angle α_f slightly decreases with increasing w/t for both grades, but on a higher level for DP600 than for CP1200/MS1300 (Figure 2).

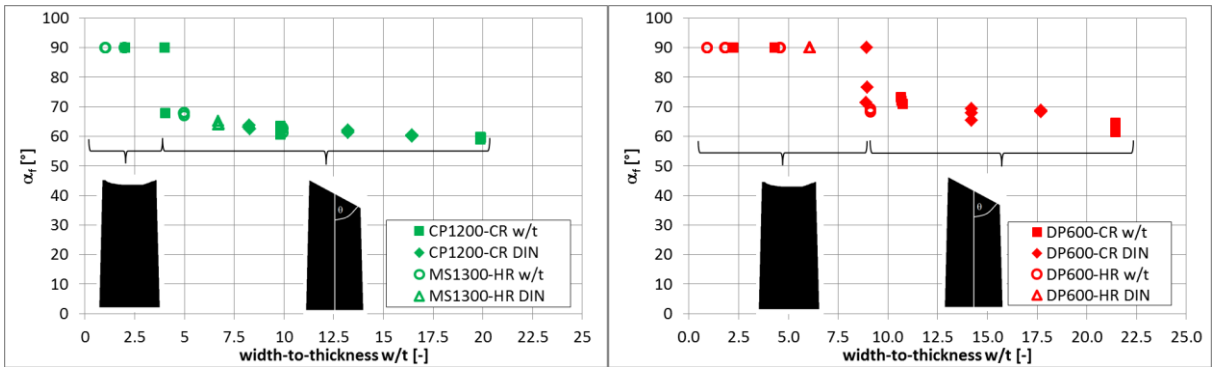

Figure 2. Change of fracture type with increasing w/t for CP1200/MS1300 (left) and DP600 (right).

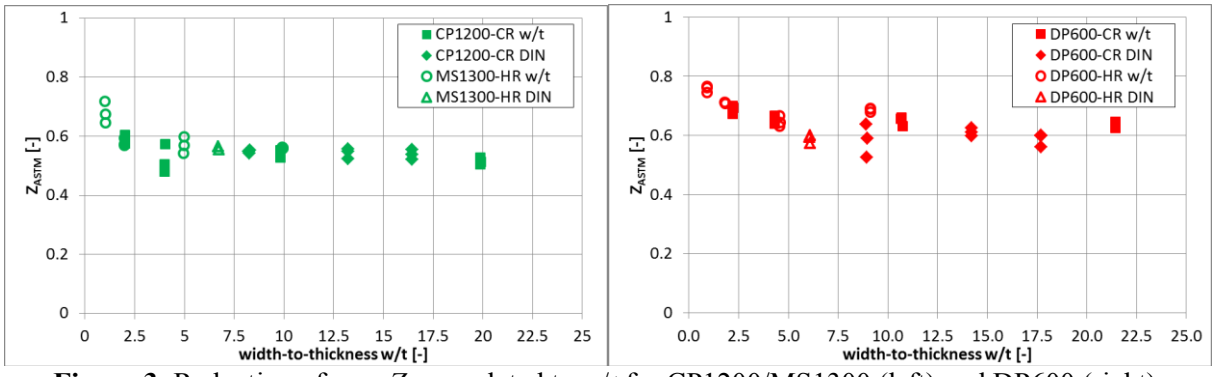

Figure 3. Reduction of area Z_{ASTM} related to w/t for CP1200/MS1300 (left) and DP600 (right).

3.1. Local Fracture Strain Measures related to w/t

The results shown here are based on A_{fASTM} (Eq. 1) as well as on t_{fMEAN}. The reduction of area Z decreases with increasing w/t until the aforementioned w/t_{CRIT}, where the fracture behaviour changes to shear fracture across the specimen width (Figure 3). For values around w/t_{CRIT} an amplified scatter is

observed. Thereafter, i.e. for *w*/*t* resulting in shear fracture, the values remain on a constant plateau. True fracture strain *TFS* shows similar behaviour, only the initial decrease for increasing *w*/*t* is more pronounced and the experimental scatter is slightly amplified (not shown).

The true thickness strain TTS_{MEAN}, i.e. based on t_{fMEAN}, shows no distinct trend for *w*/*t* below w/t_{CRIT} (Figure 4). A large scatter is again observed for values around w/t_{CRIT}, followed by a constant plateau of values, as seen for *Z* (Figure 3). True width strain TWS does again show a distinct drop with increasing *w*/*t* until w/t_{CRIT} and a constant plateau thereafter (Figure 5).

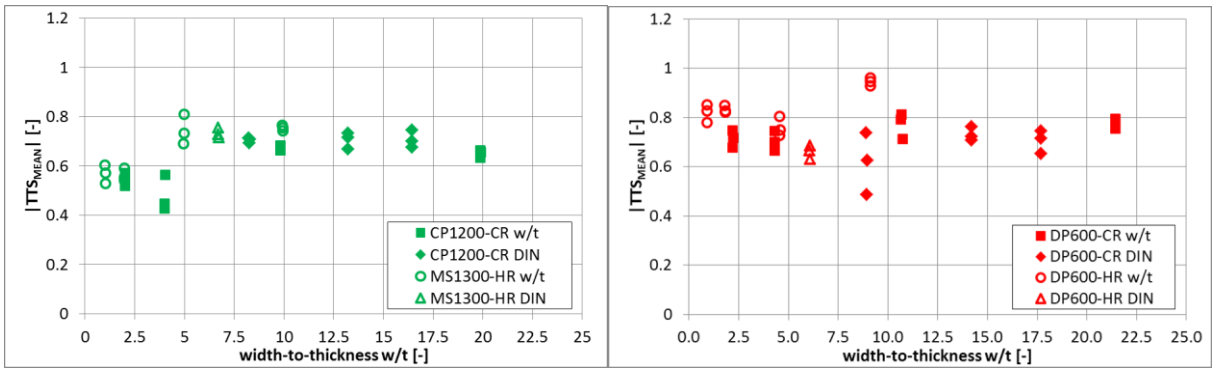

Figure 4. True thickness strain TTS_{MEAN} related to *w*/*t* for CP1200/MS1300 (left) and DP600 (right).

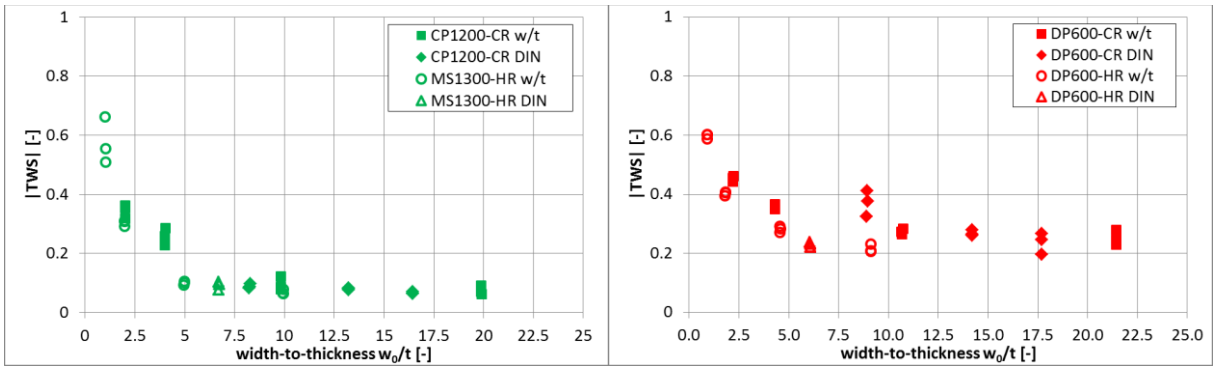

Figure 5. True width strain $TWS(w_f)$ related to *w*/*t* for CP1200/MS1300 (left) and DP600 (right).

3.2. Influence of Evaluation Method

The results shown above, based on A_{fASTM} and t_{fMEAN}, are now compared to the corresponding results from other evaluation methods. As for *Z*, the majority of values based on $A_{fContour}$ are equivalent to the corresponding values based on A_{fMEAN} (Figure 6).

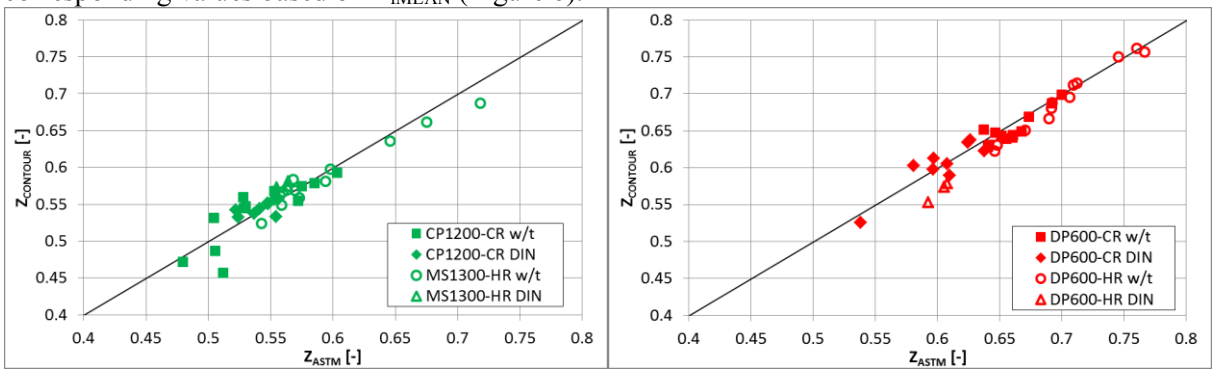

Figure 6. Reduction of area *Z* evaluated by contour measurement vs. ASTM-formula for CP1200/MS1300 (left) and DP600 (right).

Deviations can be found for w/t below w/t_{CRIT}, especially for CP1200/MS1300, where $A_{fContour} > A_{fMEAN}$. The overall trend of Z_{ASTM}, shown in Figure 3, remains also for $Z_{CONTOUR}$. Regarding TTS, it can be seen that TTS_{MEAN} is always smaller than TTS_{MIN} (Figure 7) or TTS_{MID} (not shown). This is due to the fact that t_{fMEAN} represents a weighted average thickness, including the – usually larger – edge thicknesses as well (Figure 1). For $w/t < w/t_{CRIT}$ a more or less cup and cone parabolic shape of the fracture surface can be found (Figure 1a). For $w/t > w/t_{CRIT}$ no distinct parabolic shape of the fracture surface can be found – it exhibits a rather rectangular shape with only slightly higher thicknesses at the edges (Figure 1b). Thus the difference between TTS_{MEAN} and TTS_{MIN} (as well as TTS_{MID}) is higher for samples with w/t below w/t_{CRIT}.

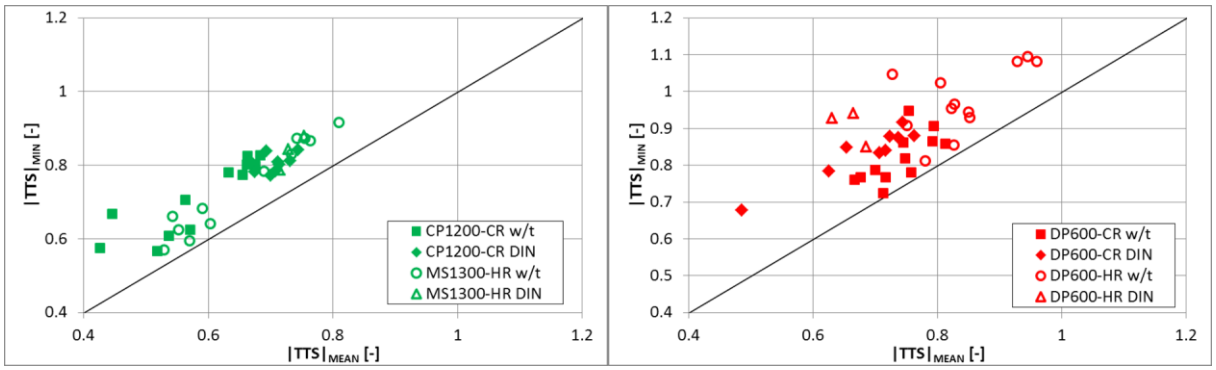

Figure 7. True thickness strain $TTS(t_{fMIN})$ vs. TTS (t_{fMEAN}) for CP1200/MS1300 (left) and DP600 (right).

3.3. Impact of Measurement Artefacts

Obviously, the accuracy of the local fracture strain measures depends on the quality of the image taken from the fracture surface. Care has to be taken to ensure using a microscope providing sufficient depth of field. This is vital especially for fracture surfaces where w/t is below w/t_{CRIT} due to the cup and cone type of fracture (Figure 2). If the depth of field is too small a compromise has to be made as regards to where to focus the image (Figure 8a,b). Areas above and below the focal plane will appear blurred and amplified to some extent. Different issue arise for samples with w/t above w/t_{CRIT}. For DP600 the shear fracture across the specimen width does not follow a straight path but is interrupted by a small ductile fracture zone in the centre of the specimen (Figure 8c,d).

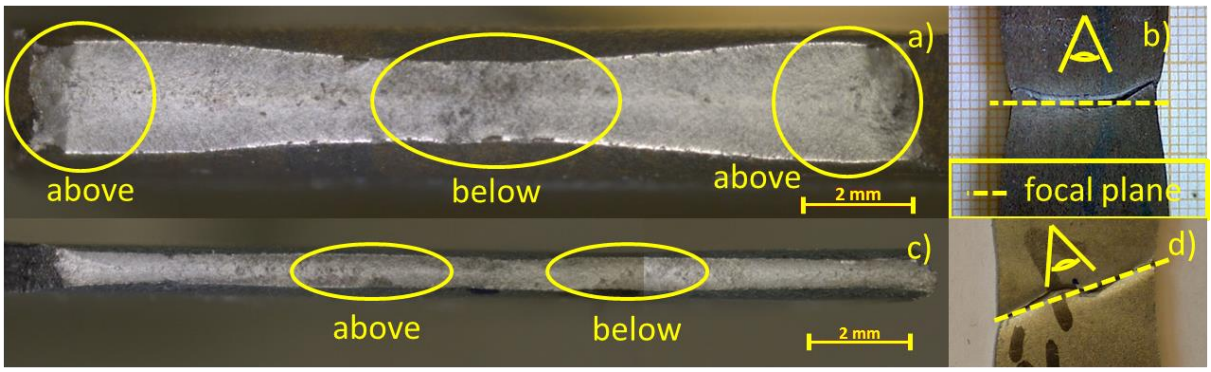

Figure 8. Focussing problems when using a microscope with insufficient depth of field.

This again leads to focussing problems as the whole fracture surface cannot be aligned perpendicular to the viewing direction. In fact the middle section of the fracture surface might even appear to show less thinning as compared to adjacent areas.

A not so obvious problem arises for samples with w/t above w/t_{CRIT} for CP1200/MS1200. Here the mode of deformation is dominated by in-plane shear just before to fracture. The resulting relative

motion of the upper and lower specimen half results in a draw in of material as well as the formation of a burr on the opposite side of the fracture surface (Figure 9). The rather undefined transition from the lateral side face of the sample towards the fracture surface (Figure 9b,d) might render the detection of the fracture surface edge impossible. The burr on the opposite side (Figure 9c,e) does not always remain with the broken specimen, it may as well be lost during fracture, reducing the measured fracture surface width w_f.

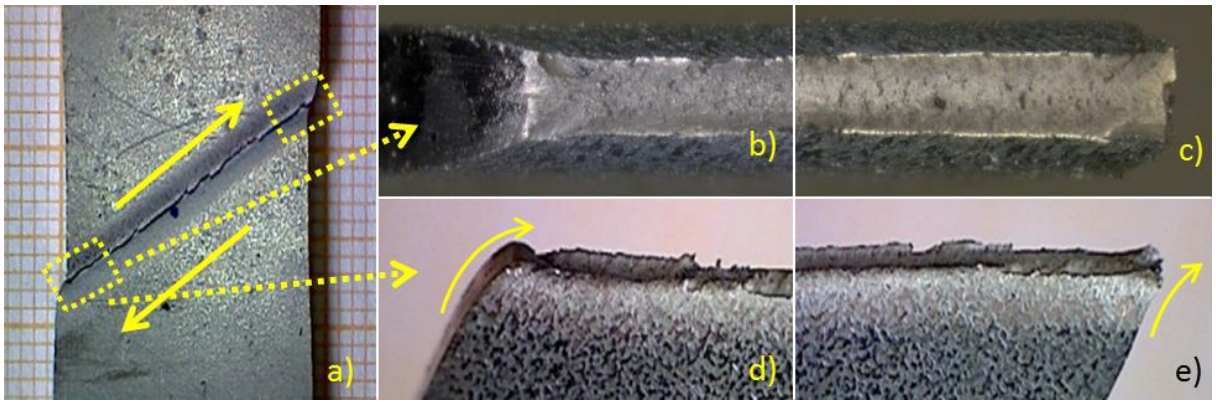

Figure 9. Effect of in-plane shear deformation prior to fracture on the resulting fracture surface.

Here the measurement of w_f might be additionally performed by means of an image of the joined fractured specimens from the top side (Figure 9a), if available. However, comparing measured w_f from cross sections to respective w_f from side images of joined specimens revealed a deviation in the order of -1.5% for CP1200/MS1300 and -0.5% for DP600, which can be regarded as negligible. In addition the slope of the fracture surface across the thickness frequently changes. This might render the detection of the actual fractured minimum cross section impossible, since the edges of the fracture surface do no longer follow the narrowest contour around the localized necking zone (Figure 10). The localized necking zone either might be preserved completely on one broken half-specimen only (Figure 10a,b), or the transition from the slopes of the fracture surface across the specimen thickness to the adjacent necking region might not be well defined (Figure 10c).

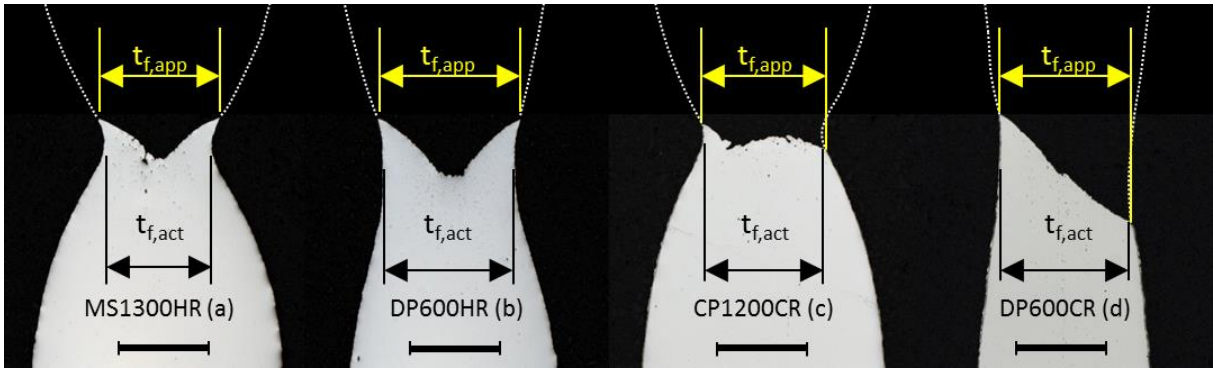

Figure 10. Apparent $t_{f,app}$ and actual fracture thickness $t_{f,act}$ measured in the necking region; scale bars: a-b – 1mm, c-d – 0.5mm; images perpendicular to sheet plane and fracture surface; dotted lines give an imagination of the opposite specimen half constructed from mirrored outlines.

While this effect does again not play a big role for sheet thickness of 1.5mm – with $t_{f,act}$ differing from $t_{f,app}$ by less than 1.5% – it does affect the thickness measurement for sheet thickness of 3.0mm – with $t_{f,app}$ being up to 13% higher than $t_{f,act}$.

4. Conclusions

Depending on the tested steel grade and thickness, the choice of test specimen may have an influence on the reported local fracture strain measures. To gain stable values it seems to be necessary to choose

specimen geometries such that the resulting width-to-thickness ratio w/t is large enough to result in a shear fracture across the specimen width. This critical w/t_{CRIT} is a material-specific parameter, i.e. depending on the strain hardening behavior. Surface-based local fracture measures, i.e. *Z*, *TFS*, tend to yield less experimental scatter as compared to length-based local fracture measures, i.e. *TTS*. In addition, surface based measures show smaller dependence on the method of fracture surface assessment, as compared to the dependence of length-based measures on the determination of the fracture thickness. Thus, to ensure viable reproducibility we advise to use surface based local strain measures or at least use some kind of averaging of measured fracture thicknesses to determine thickness based local strain measures. This will also ensure that the stochastic nature of fracture is accounted for, i.e. both actual or apparent local minima or maxima in fracture thickness will not distort the formability assessment of the investigated AHSS grade. Furthermore it is suggested that at least three parallel tests with statistics-based outlier elimination are performed in order to gain reliable overall information on material fracture behavior.

References

[1] Hance B M and Davenport M D (2016) AHSS: Deciphering Local and Global Formability. Int. Automotive Body Congress, Sept. 28-29, Dearborn, MI, USA.
[2] Larour P, Freudenthaler J and Weissböck T (2017) Reduction of cross section area at fracture in tensile test: measurement and applications for flat sheet steels. Journal of Physics: Conference Series 896, 012073.
[3] VDA 239-100 (2016) Material specification - Sheet Steel for Cold Forming, Verband der Automobilindustrie e.V.
[4] Keeler S, Kimchi M and Mooney P J (2017) Advanced High-Strength Steels Application Guidelines Version 6.0, WorldAutoSteel, pp. 3-16, April. http://www.worldautosteel.org
[5] ISO 6892-1:2009 (2009) Metallic materials - Tensile testing. European Committee for Standardization, Brusseles, Belgium.
[6] ASTM E8/E8M-15a (2015) Standard Test Methods for Tension Testing of Metallic Materials. ASTM International, West Conshohocken, PA, USA.
[7] JIS Z 2241 (2011) Metallic Materials – Tensile Testing – Method of Test at Room Temperature. Japanese Standards Association, Tokyo, Japan.
[8] Zhang Z L, Hauge M, Ødegård J and Thaulow C (1999) Determining material true stress-strain curve from tensile specimens with rectangular cross-section. International Journal of Solids and Structures 36, p.3497-3516.